ELSEVIER

Chemical Engineering Journal 128 (2007) 141–154

Chemical Engineering Journal

www.elsevier.com/locate/cej

"Paradox" of flow reversal caused by protective wall-jet in a pipe

V. Tesař*

Department of Chemical and Process Engineering, The University of Sheffield, Sheffield, UK

Received 4 April 2006; received in revised form 31 July 2006; accepted 7 October 2006

Abstract

Some fluids must not come into direct contact with solid walls, from which they have to be separated by a co-flowing wall-jet of protective fluid. In a pipe with the faster wall-jet at the wall, the core flow may be expected to be move faster. After all, the wall friction is eliminated and the radial momentum transport from the wall-jet towards the axis may be expected to increase the central flow velocity. What actually happens is the very opposite: the central flow is slowed down and may even reverse its direction so that it flows upstream, against its original directions as well as the direction of the wall-jet. This unexpected reversal was found [V. Tesař, 1978–1980] in radioactivity detectors. Early simple measurements and contemporary hypothesis about its origin (entrainment into the wall-jet) were recently vindicated by numerical flowfield computations. These were performed in a more general way, for a whole family of related geometries, and provide an input information for an analytical model based on control volume balance. The resultant control volume model is useful for designing devices using wall-jet flows in a confined space.

Keywords: Protective fluid film; Wall-jet; Recirculation; Radioactivity detection; Flow reversal

1. Introduction

Recent renewed interest in nuclear energy as one of the few available actions capable of decreasing the global warming has led to revival of investigations of radioactivity detection and monitoring. Of particular interest is monitoring of fluid flows leaving the radioactive or possibly activated space. The fundamental problem of all radioactivity measurements is the possibility of activation of the detector itself or nearby objects. To prevent it, the test section of the duct guiding the tested fluid is often provided with a protective "fluid film", a fast co-flowing wall-jet of non-radioactive fluid blown along the walls.

Interestingly, early tests of such a device for monitoring radioactivity of air flow in a pipe, to the dismay of its original designers, revealed that the protective parallel wall-jet blown along the pipe wall can generate aerodynamic effects which contradict a simple reasoning. The tested fluid may be quite legitimately expected to flow faster since the wall friction is eliminated by the presence of the wall-jet. Moreover, the wall-jet may be expected to accelerate the tested main flow by the inevitable radial gradient transport of axial momentum from the faster fluid to the slower one. However, the experiments have shown the very opposite effect. The admission of the fast wall-jet actually slows down the central flow of the tested fluid. It can even cause it to reverse its direction so that near the pipe axis it flows upstream—against the axial pressure gradient and against the original directions of both central flow as well as the wall-jet.

2. Protective "guard" flow

A typical case of the fluid flow radioactivity monitoring is the detection of possible leaks from furnaces used for encapsulation of radioactive waste into glass. The furnace effluents are normally neutral and may be released to the atmosphere. The flow, however, must be continuously monitored by a detector placed into the pipe that carries the effluents. The design problem is that the effluents must not come into contact with the pipe wall in the vicinity of the detector. Should they do so, pipe wall may become radioactive during a leakage event, making it later impossible to tell whether the subsequently measured radioactivity levels are due to actual contamination of the effluent gas or come from the activated walls. The solution is to use protective "guard" flow at the wall. In the furnace case, the radioactivity in question is the short-range α activity so that the walls are sufficiently protected even by a quite thin "film" of clean gas (air)

* Present address: Institute of Thermomechanics, Academy of Sciences of the Czech Republic, Dolejskova 6, 182 00 Prague, Czech Republic.
E-mail address: v.tesar@sheffield.ac.uk.

1385-8947/$ – see front matter © 2006 Elsevier B.V. All rights reserved.
doi:10.1016/j.cej.2006.10.007

Nomenclature

A	area of nozzle exit (m^2)
b	nozzle slit width (m)
c_f	friction coefficient
D	pipe diameter (m)
d	nozzle internal diameter (m)
Eu_M	Euler number
F_f	friction force (N)
H_{X_1}	nozzle exit nozzle exit shape factor
H_{X_2}	central flow shape factor
H_Y	critical section shape factor
$\dot{M}_{X_1}$	nozzle exit mass flow rate (kg/s)
$\dot{M}_{X_2}$	main mass flow rate (kg/s)
ΔP	pressure rise (Pa)
Re	Reynolds number
Re_b	nozzle exit Reynolds number
v	specific volume (m^3/kg)
$\bar{w}_1$	time-mean axial velocity (m/s)
w_a	velocity on pipe axis (m/s)
$\dot{W}_{X_1}$	axial momentum flow rate at nozzle exit (N)
w_{X_1}	bulk velocity in nozzle exit (m/s)
$\dot{W}_{X_2}$	axial momentum flow rate of the central flow (N)
w_{X_2}	bulk velocity of the central flow (m/s)
$\dot{W}_Y$	momentum flow rate in the critical section (N)
X_1	axial position (m)
X_{sd}	axial distance of downstream stagnation point (m)
X_{su}	axial distance of upstream stagnation point (m)

Greek letters

φ	area ratio
μ_e	flow ratio
σ_s	relative distance of the critical point
τ_w	wall shear stress (N)

issuing from a thin slot upstream from the detector and covering the walls of the test section, as shown in Fig. 1.

A through-flow cuvette with the protective air film, laid out along the lines of the schematic Fig. 1, was designed and tested in 1978 for the Institute of Nuclear Research in Řež near Prague, Czech Republic. The tests revealed a surprising effect. The detector signal indicated a prolonged presence of radioactive substances inside the cuvette for considerable time after the seeding of radioactive test aerosol into the gas ceased. The signal gradually decreased but the decay was in no relation to what would be a much longer half-time of the radioactive particles or the possibly activated test pipe material. In fact, subsequent measurements proved that walls were not activated and the protective wall-jet carried out its task as planned.

The unexpected response was obviously due to temporary hold-up of the radioactive aerosol inside the tube, somewhere in the immediate vicinity of the detector—as was apparent considering the short-range of the radiation. The cuvette there, however, was a plain constant cross-section round tube with no obvious traps or baffles capable of creating any dead zones. The captive radioactivity remained in the pipe near the detector despite a generously increased flow rate of the protective air jet, which was expected to facilitate removal of the sample away from the pipe. Quite surprisingly, the increase in the protective gas flow rate, instead of helping to remove the aerosol, enlarged the amount held inside the cuvette.

The effect was described as “reversation paradox”. It was explained (Tesař [4]) as a consequence of entrainment into the protective wall-jet—an entrainment so strong that it exceeds the available supply of fluid from the upstream part of the pipe. A conjectured consequence was the presence of a recirculation bubble which forms on the pipe axis by the returning flow entrained into the wall-jet. Because of scarcity of experimental data, this explanation was in [4] formulated only as a hypothesis. Its existence was later proved by numerical flowfield computations and included in Fig. 1 is an example of the computed flow reversal region.

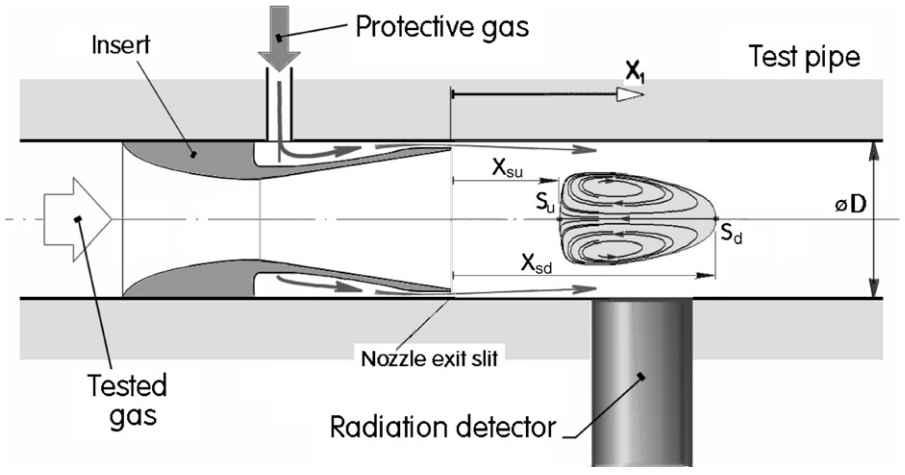

Fig. 1. Schematic representation of the test pipe with the protective gas film injection immediately upstream from the radiation detector. Also shown is a typical computation result (for the geometry shown in Fig. 2) with the pathlines defining a stationary recirculation bubble surrounding a stationary vortex ring.

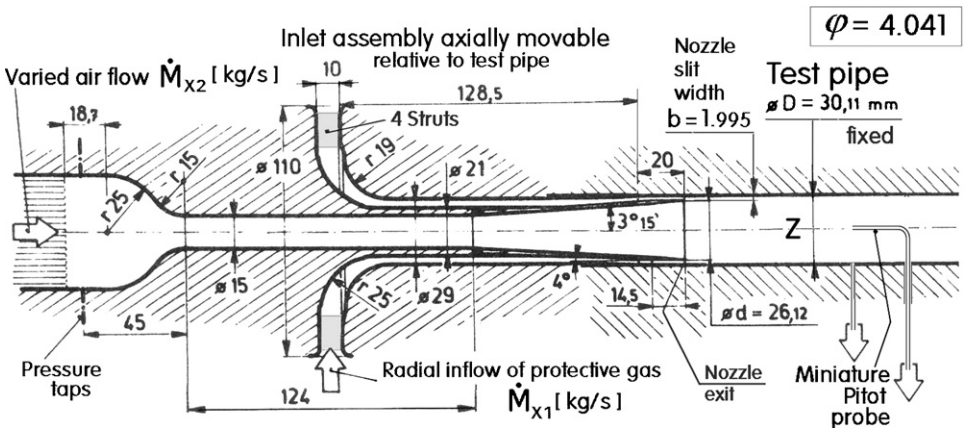

Fig. 2. Geometry of the experimental test set-up as well a numerical flowfield computations. In the experiment, the Pitot probe was fixed to the pipe. To change its axial distance X_1 from the wall-jet nozzle exit (defined in Fig. 1), the inlets (for central flow as well as for the wall-jet, fixed together) were moved into different distances inside the pipe entrance.

A similar phenomenon certainly can take place in other devices using high-speed wall-jets in a confined space. In the jet pumps with an annular driving jet, this recirculation certainly also takes place in some operating regimes, though it apparently escaped attention in literature. The fluid film wall protection used in chemical engineering practice and cooling gas films of combustion chambers are other examples of the situation where the recirculation bubble is likely to form and to be important. In the cuvettes, it should be avoided while in some other applications the baffle-less retention of the fluid inside the pipe may be a welcome useful effect. Because of the potential usefulness of similar devices it is considered beneficial to set up an analytical model of the phenomenon making possible a prediction of the flow reversal. Apart from understanding of the effect, the model provides a useful relation between the individual parameters so that anyone designing a similar device can either avoid or secure the presence of the flow reversal.

3. Early experimental investigation

When the present author investigated the surprising fluid retention phenomenon in 1978–1980 [4], he faced several problems. At that time, neither hardware nor software for flowfield computation were available in the then socialist countries. Indeed, even proper publication of the results was not possible due to the highly secretive nature of all nuclear research. Instrumentation for flowfield studies was limited practically to Pitot probes. The author made himself a miniature Pitot probe from a hypodermic needle and used it – together with the static pressure tap on the pipe wall – to measure velocity distribution along the pipe axis at various axial distances X_1 (Fig. 1), in particular to locate the axial positions at which the flow direction undergoes its reversal. One of the problems was the difficult access into the internal space of the pipe. Instead of the axial movement of the probe, difficult to set up, the probe was fixed to the test pipe and its axial distances were changes by moving axially the nozzle from which issued the wall-jet, together with the central inlet so that the geometry of the inlet components remained identical. Details of the experimental rig are presented in Fig. 2.

Like all paradoxes in fluid mechanics, also this "reversation paradox" (Tesař [4]) is easily explained. Nevertheless, it was quite stunning to find the axial flow oriented opposite to the directions of both the main central flow as well as of the protective wall-jet, which was intended and expected to facilitate the flow into the positive X_1 direction. Not only the velocities in the return flow region were negative relative to the axial pressure gradient in the pipe. Perhaps equally surprising were their high absolute magnitudes, much higher then the velocities on the axis of the test pipe elsewhere, either upstream or downstream.

In the experiments with the rig shown in Fig. 2 the attention concentrated on measuring the extent of the reversed flow and on the conditions under which it ceased to exist. The collected data were the positions of the two stagnation points, S_u upstream and S_d downstream, as shown in Fig. 1. Their locations vary with the ratio of the two inlet flows, the main flow rate $\dot{M}_{X_2}$ and the protective wall-jet flow rate $\dot{M}_{X_1}$. The definition of the flow ratio in [4] attributed the negative sign to this ratio to bring the sign convention in line with the usage in jet pumping:

$$\mu_e = -\frac{\dot{M}_{X_2}}{\dot{M}_{X_1}} \tag{1}$$

Admittedly, the Pitot probe is not ideally suitable for locating the position where the velocity changes sign. The probe properties are asymmetric, it cannot reasonably measure negative velocities (directed opposite to the positive direction of X_1 axis, Fig. 1). As a result, the stagnation point positions were not found very reliably. The wall pressure tap, justified in parallel flow in a pipe, fails to function properly in the present case where there are local radial flows near the stagnation points, with which are associated (fortunately, as later computations have shown, not very strong) radial pressure gradients.

Nevertheless, even accounting for the possible errors, the basic fact of existence of the return flows on the axis was established beyond doubt and also the general character of the dependence of the stagnation point location on the relative magnitude of the wall-jet flow μ_e was established reliably. The results of the experiments are plotted in Fig. 4. The conjectured separation bubble corresponding to the region of negative velocity on the

axis was found to move upstream and grow in size with increasing intensity of the protective jet flow—i.e. decreasing absolute value of the ratio μ_e.

Important for the applications is the fact that the recirculation region disappears if the magnitude of the jet flow intensity, characterised by the absolute value of μ_e, is above a certain critical value, in [4] measured – possibly not very reliably – to be,

$$\mu_{e\ crit} = -0.732 \quad (2)$$

Unfortunately, these results could not be properly published and in the meantime became practically forgotten.

4. Explanation of the effects and related flows

To explain the flow reversal, it is useful to consider related flows. Some of them may be obtained in the configuration described above if the flow parameters are varied beyond the usual limits.

First, it is apparent from Fig. 4 that the recirculation bubble size grows with diminishing magnitude of the central main flow. It may be interesting to consider the limiting case of zero central flow. The bubble, which then reaches its maximum extent, in fact becomes a wake attached to the central inlet. The flowfield then corresponds to a flow past a solid axisymmetric body held inside the pipe. Character of the wake on the downstream side of such body is well known. Nothing surprising is associated with the reversed, upstream-directed flow in the wake. The flowfield of present interest differs only by the non-zero central flow, which separates the wake from the nozzle lips of the inlet. The separation is understandable: the central flow, which has to get somehow into the stream-wise direction, cannot pass through the wake. It bypasses the wake on its periphery, at the nozzle exit lips where the local wake flow has the same streamwise orientation. The mental steps from the wake case to the present confined wall-jet case provide a natural explanation to the observed effects.

The second approach to the explanation is based on considering the opposite change of the main central flow increasing in intensity. When its velocity becomes higher than that of the wall-jet, the latter, of course, would cease to be a wall-jet. The resultant flowfield becomes what is known as the confined jet flow, known and studied for more than a half of the century, since the work of Thring and Newby [1] on combustors and the systematic investigations of Craya and Curtet [2]. Confined jet has many practical applications in jet pumping, combusting furnace flows, arterial blood flows, and ventilation of lungs and has, therefore, been frequently studied and well understood. Its important feature is formation of a recirculation region by a mechanism analogous to what is found in the flow of present interest. Because of the "inverted" configuration, with the slower flow on the wall side, the recirculation region is attached to the pipe wall. Its core is of toroidal shape [8,10] as in the present case, but rotating in the opposite sense. Again, this recirculation region forms if the jet entrainment demands cannot be satisfied by the secondary slower inflow—in the confined jet case it is an entrainment into the central jet from the outer annular co-flow. This recirculation effect, well known and accepted for the confined jet case, requires just the logical step of inverting in the meridian plane the conditions at the wall and at the pipe axis to explain the discussed "paradox".

In the confined jet flows, there are already established parameters in use for characterisation of the flowfield. Thring and Newby [1], in their combustor studies, applied physical and dimensional reasoning to the problem of hydrodynamic similarity between a combustor and its laboratory model. They derived a single non-dimensional similarity parameter, the Thring–Newby number. The recirculation region should be found in the confined jet flow whenever this number reaches a critical value. For the simplified model situation of flat velocity profiles the Thring–Newby number can be shown to reduce to the square root of the ratio of the momentum flow rate of the exit flow to that of the central jet. Recent studies [8] have actually shown this to be an incomplete, approximate similarity. They indicated as a deficiency of the Thring–Newby number its failure to include the influence of the momentum flow rate of the secondary inlet flow. In the combustor applications of Thring and Newby this influence was not recognised because the annular secondary air flow there has usually low momentum in relation to the burner central jet flow.

Barchilon and Curtet [3] later arrived at a different similarity parameter, the Craya–Curtet number. Its generalised version was recently introduced by Foster et al. [8]. An inconvenient feature of the Craya–Curtet number is its definition involving integrals of velocity, of velocity squared, and of pressure distributions over the inlet plane. As a result, this number can be evaluated by integration only *ex post*, when processing data of an experimentally investigated or computed flow. The parameter is, therefore, of only limited use for early stages of a device design or other situations where the distributions are not known. Under the simplified situation of constant pressure, constant velocity profiles in the two inlets, the Craya–Curtet number reduces to the square root of the ratio of the momentum flow rates of the inlet outer annular flow to that of the inlet central flow (some authors, e.g. Revuelta et al. [10], wrongly assume this to be the actual definition of the number). Computed confined jet flow results are available for the simple laminar flow case [10] and for turbulent flows modelled by the k–ε model [8] demonstrating the similarity – albeit only approximate – of the confined jet case and, therefore, at least approximate predictability of the presence of the recirculation region.

5. Analytical model

The aim of the present paper is to set up a theoretical model – perhaps only approximate but as far as possible universal – of the flow with the fast wall-jet and the axially positioned recirculation bubble in a circular pipe. In particular, the theory is to be useful for the renewed interest in radioactivity measurements of flowing fluids. This re-kindled the old problem of possible radioactive particle retention in the recirculation bubble in detectors with the protective wall-jet. The advantage of the mathematical model is its capability of providing device designers – or anyone seeking deeper understanding of the flow reversal

phenomenon – with a guidance as to the existence of the recirculation bubble for given device dimensions and flow rates. Of course, the universality is limited by the impossibility of taking into account various possible inlet geometries. However, even though the inlet shapes may differ from one case to another, their influence is under typical conditions only secondary and may be accounted for by profile shape parameters, characterising the deviations from the simplified constant velocity, constant pressure profiles in the plane of the nozzle exit. Analysis of the investigated case, based on extensive set of numerical flowfield computations, is intended to provide some guidance about the numerical values of the parameters.

Further downstream from the nozzle exit plane, cross-section of the pipe is assumed to be of constant diameter. This simple shape means that the geometry of the interaction region is sufficiently determined by a single scalar-valued parameter—the area ratio φ. It is here defined as the ratio of the cross-sectional area of the pipe $\pi D^2/4$ to the nozzle exit cross-section area A:

$$\varphi = \frac{D^2}{4b(D-b)} \tag{3}$$

where D (m) is the pipe diameter; b (m) is the nozzle slit width – Figs. 1 and 2.

The most important fact, which the discussed theory is expected to predict, is the existence of the flow reversal. This is determined by predicted ratio of the inlet flows at which occurs the critical state—the situation when the volume of the recirculation bubble reduces to zero so that the two stagnation points X_{su} and X_{sd} coincide. The conditions in this single point not only represent a theoretically interesting flowfield with an isolated zero-velocity point. They are of practical importance. The critical value $\mu_{e\,crit}$, of the ratio μ_e of the two input flows is the boundary beyond which the reversal phenomenon cannot complicate the operation of the radioactivity detector or similar devices, like the annular primary nozzle jet pump. The essential point of the theory is, therefore, its ability to predict the dependence:

$$\mu_{e\ crit} = f(\varphi) \tag{4}$$

The idea to base the theory on one-dimensional balance of axial momentum flow rates at the boundaries of the control volume positioned between the inlet X and the critical state at the downstream location Y was introduced by Markland in a memorandum [5] which, unfortunately, was never published. Some Markland's assumptions, made at a time when there was no information about the shapes of the velocity profiles, are now known to be wrong. Nevertheless, the basic idea is worth following. For the control volume shown in Fig. 3, the force balance condition may be written as

$$\dot{W}_{X_1} + \dot{W}_{X_2} = \dot{W}_Y + \Delta P \varphi A + F_f \tag{5}$$

where $\dot{W}_{X_1}$ (N = kg m/s^2) is the axial component of momentum flow rate at the nozzle exit X_1, $\dot{W}_{X_2}$ (N) is the axial component of momentum flow rate at the central, main flow inlet X_2, $\dot{W}_Y$ (N) is the axial component of momentum flow rate in the pipe cross-section passing through the critical point Y, ΔP (Pa) is the pressure rise between X (assuming pressure in X_1 to be the same as in X_2) and Y, A (m^2) is the cross-sectional area of the wall-jet nozzle exit, and F_f (N) is the friction force acting on the pipe wall between the locations X and Y.

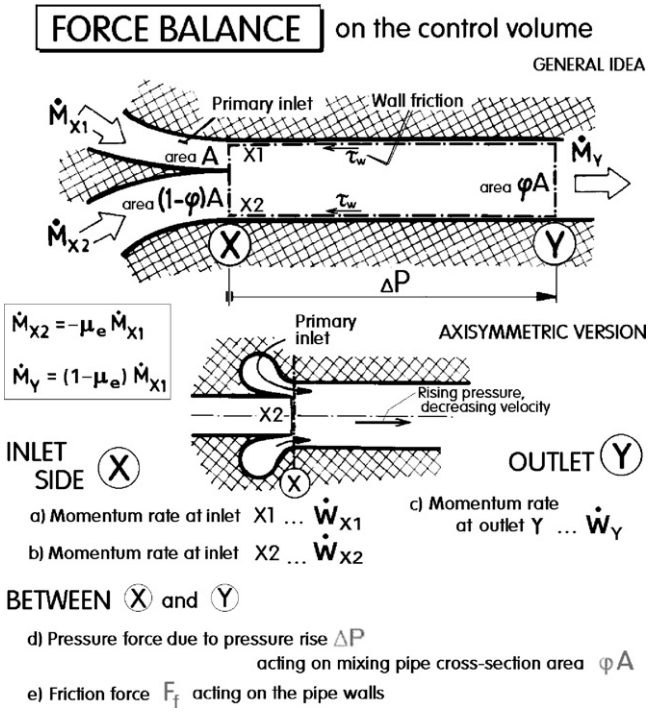

Fig. 3. The general basic relations for mixing the two inlet (X) flows of the same fluid and the condition for the critical state at a downstream location (Y) following from momentum rate, pressure, and friction force balance.

The control volume analysis would be very easy if it were acceptable to assume uniform velocity profiles. For example the momentum flow rate $\dot{W}_{X_1}$ in the wall-jet nozzle X_1, where the mass flow rate $\dot{M}_{X_1}$ issues through the nozzle exit of cross-section area A, could be under the assumption of the uniform velocity profile evaluated as

$$\dot{W}_{X_1} = \frac{v}{A}\dot{w}^2_{X_1} \tag{6}$$

where v (m^3/kg) is the specific volume of the fluid, a constant in the assumed incompressible flow regime. Similarly, the value $\dot{W}_{X_2}$ in the central main inlet X_2 would be

$$\dot{W}_{X_2} = \frac{v}{A(\varphi-1)}\dot{M}^2_{X_2} \tag{7}$$

and also $\dot{W}_Y$ in the control volume outlet Y would be evaluated in an analogous manner. The actual profiles, however, are more complex. The deviation from the simple uniformity in the case of inlet X_1 is caused by the boundary layers developing on the nozzle walls (cf. [9]). The uniformity assumption is even much less acceptable for the central main flow in the inlet X_2, especially if, as is usual the case, the device designer places (Figs. 1 and 2) the annular nozzle into the internal space of the pipe. This leads to shaping the central channel as a conical diffuser—a device known to produce velocity profiles with high-velocity central peak and low-velocity flow near the wall. Finally, the uniform

profile assumption is quite obviously unacceptable in the control volume outlet Y. The velocity there must be zero on the pipe axis as well as at the wall.

The deviations of the real profiles from the simplified uniform shape may be formally expressed by introducing the shape parameters (or shape factors) H, defined

$$\dot{W}_{X_1} = H_{X_1}\left(\frac{v}{A}\right)\dot{M}_{X_1}^2 \tag{8}$$

$$\dot{W}_{X_2} = H_{X_2}\left(\frac{v}{A}\right)\frac{\mu_e^2}{\varphi-1}\dot{M}_{X_1}^2 \tag{9}$$

and

$$\dot{W}_Y = H_Y\left(\frac{v}{A}\right)\frac{(1-\mu_e)^2}{\varphi}\dot{M}_{X_1}^2 \tag{10}$$

The pressure rise ΔP between the cross-sections X and Y may be evaluated using Markland's [5] assumption of loss-less conversion from the fluid kinetic energy on the axis of the main inlet X_2. It may be characterised by introducing the Marklandian Euler number Eu_M:

$$v\Delta P = Eu_M\frac{v^2}{2(\varphi-1)^2A^2}\dot{M}_{X_2}^2 = Eu_M\frac{v^2\mu_e^2}{2(\varphi-1)^2A^2}\dot{M}_{X_1}^2 \tag{11}$$

Finally, the friction force may be expressed using the concept of the wall shear stress τ_w averaged over the pipe wall surface on the distance $X_S = \sigma_S D$ between the sections X and Y,

$$F_f = \tau_w\sigma_S\pi D^2 = 4\tau_w\sigma_S A \tag{12}$$

and characterised by friction coefficient c_f, relating it to the dynamic pressure in the annular nozzle exit:

$$v\tau_w = c_f\frac{1}{2}\left(\frac{v}{A}\right)^2\dot{M}_{X_1}^2 \tag{13}$$

The resultant force balance condition, by using these expressions as the terms in Eq. (5), is

$$\begin{aligned} &H_{X_1}\left(\frac{v}{A}\right)\dot{M}_{X_1}^2 + H_{X_2}\left(\frac{v}{A}\right)\frac{\mu_e^2}{\varphi-1}\dot{M}_{X_1}^2 \\ &= \left(\frac{v}{A}\right)Eu_M\frac{\varphi\mu_e^2}{2(\varphi-1)^2}\dot{M}_{X_1}^2 \\ &\quad + H_Y\left(\frac{v}{A}\right)\frac{(1-\mu_e)^2}{\varphi}\dot{M}_{X_1}^2 + 2c_f\sigma_S\left(\frac{v}{A}\right)\dot{M}_{X_1}^2 \end{aligned} \tag{14}$$

This equation may be used as the condition for the existence of the critical state (flow slowing down to zero-velocity at a single point on the pipe axis). It is useful to non-dimensionalise its terms by dividing them by the idealised momentum flow rate in the annular nozzle entrance, Eq. (6). The resultant dimensionless control volume force balance:

$$\begin{aligned} &H_{X_1} + H_{X_2}\frac{\mu_e^2}{\varphi-1} \\ &= Eu_M\frac{\varphi\mu_e^2}{2(\varphi-1)^2} + H_Y\frac{(1-\mu_e)^2}{\varphi} + 2c_f\sigma_S \end{aligned} \tag{15}$$

with $\mu_e = \mu_{e\,crit}$ is the sought-after relation Eq. (4). With respect to $\mu_{e\,crit}$ it is a quadratic algebraic equation so that

$$\mu_{e\ crit} = \frac{-b+\sqrt{b^2-4ac}}{2a} \tag{16}$$

where there are

$$a = \frac{H_{X_2}}{\varphi-1} - \frac{Eu_M\varphi}{2(\varphi-1)^2} - \frac{H_Y}{\varphi} \tag{17}$$

$$b = 2\frac{H_Y}{\varphi} \tag{18}$$

$$c = H_{X_1} - \frac{H_Y}{\varphi} - 2c_f\sigma_S \tag{19}$$

To be useful, these results require knowledge of the parameters $H_{X_1}, H_{X_2}, H_Y, Eu_M$ and c_f. In general, values of the shape parameters H should be near to 1.0—significant deviations from this value indicate the theory is not successful. In the initial designs stages of the devices it may be acceptable to estimate roughly their values as slightly higher than $H \sim 1.0$ to get at least some idea about the device operation—to be later corrected, especially if the profiles exhibit a local high-velocity peak, to the values at which the parameters are sensitive due to the quadratic dependence on the velocity.

So far, the lack of information about the five dimensionless parameters has been the main obstacle to further progress. To evaluate them requires a knowledge about the investigated flowfield.

6. Numerical flowfield computations

The experimental rig used by this author was scrapped long time ago and could be no more used to obtain the needed information. Fortunately, availability of high performance CFD hardware and software made it possible to obtain useful information by numerical flowfield computations. To provide data for the desirable general character of the theory, the computations were conceived more widely than just verification of the earlier experiments. They covered a range of seven geometries characterised by values of the area ratio φ from 3.28 to 5.28.

This represented quite demanding computation effort. To map reliably the extent of the recirculation region, the solutions have to be repeated at each φ value for a quite large number input flow rates, the change of which has led to the changing flow ratio μ_e. In particular, the solution runs were repeated with rather small increment steps near the critical state so as to identify reliably the critical value $\mu_{e\,crit}$.

The computations were performed in two series. The first series A used a fully three-dimensional computation domain, applying to it the three-dimensional version of FLUENT 6. The solution domain in fact did not completely disregard the axial symmetry and represented a 90° quadrant sector between two perpendicular symmetry planes passing through the axis. It used unstructured discretisation grid with 160,924 tetrahedral cells and 42,993 nodes. The three-dimensional character made possible inclusion of such small details as the four struts, which in the experiment held the central inlet part. The struts (of streamlined

shape) were small and sufficiently far upstream from the nozzle (Fig. 2) for their small wakes becoming practically unimportant before the flow entered the actual flow interaction region inside the pipe. The experience with the series A has shown that the computation runs were too time consuming. After all, no significant three-dimensional effect were found. In the second, more extensive computation series B, the economy of computation effort necessitated to use a two-dimensional (fully axisymmetric) model domain. A typical two-dimensional solution used 32,782 triangular cells with 17,455 nodes. Of course, despite this smaller numerical value, the grid cells were smaller than in the series A, being wholly contained within a plane rather than in a spatial domain. Individual computation runs actually used a different final numbers of cells, because the grid was adapted in the course of the solutions by refinement and coarsening dependent on the computed values of local absolute velocity gradient. The two-dimensional and three-dimensional solutions used a different version of the FLUENT 6 solver.

The procedure used to set up the computation models of different area ratio values φ applied to the computation series B consisted of placing the symmetry axis at different transversal distances from the otherwise identical the two-dimensional contours. Since the shape of the domain contour in the radial plane did not change, all computed configurations shared the same wall-jet inlet geometry—the geometry of the original experimental rig. All of them possessed the same nozzle exit width $b = 1.995$ mm. The area ratio φ – ratio of pipe cross-section area to the cross-sectional area of the nozzle exit slit, Eq. (3) – varied due to the changes of the diameters D from $\varphi = 3.28$ (nozzle occupying ∼30% of the smallest-sized pipe, $D = 24$ mm) to $\varphi = 5.28$ (with nozzle annulus covering only ∼19% of the largest $D = 40$ mm pipe area). This range, of course, included the value $\varphi = 4.041$ used in the originally investigated geometry of the experiment (Fig. 2).

Despite the same contour shape, because of the different transversal curvatures at the different radii, the nozzle geometry of individual family members was not identical. Also not identical were their inlet area at which the velocity boundary condition was defined. To avoid consequent large changes of the nozzle exit Reynolds number, the velocity at the boundary conditions was progressively increased with the increasing pipe diameter D, though this did not lead to Re exactly the same. Evaluated as usual from the dominant, smallest cross-section conditions (those in the wall-jet nozzle exit), all Re values were higher than $Re = 2000$. This is large enough for the flows being classifiable as sufficiently developed turbulent regimes, where the Reynolds number effects are not significant. Because of the exceptionally large overall computation effort, it was not feasible to include in this study also a systematic investigation of the effects of Reynolds number effects independent of the influence of the area ratio φ.

Numerical solutions of recirculation regions are notoriously known to be the least reliable among fluid flow computations, being strongly dependent on fine details of the used turbulence model and other features of the flowfield modelling. In the present study, the exceptional computation effort required, due to the large number of handled computed cases, did not allow using a very sophisticated turbulence-closure model. The solutions were performed with the standard two-equation k–ε model with the renormalisation group (rng) handling of regions with low Reynolds numbers of turbulence. This was a choice of necessity. Chen et al. [7] computed a closely related problem – a wake behind a body in a pipe with different but essentially similar recirculation bubble – using three alternative turbulence-closure models, including also the two-equation k–ε mode, and found this simplest one among the tested alternatives to be predictably the least successful. However, the demanding conditions in these flows resulted in no one of the three models being completely satisfactory. The other two models, requiring much more computation effort, did not perform very much better. In fact, Risso and Fabre [6] found the related confined jet flows a particularly testing case for deeper studies of turbulence. On the other hand, the same k–ε model as in the present study was recently used, e.g. by Foster et al. [8] in the quite successful computational study of the related confined jet flows. The use of the computationally less intensive model in the present case was justified by the overall aim. It was mainly acquiring information about qualitative character—especially, of the general character of the shape of the velocity profiles so as to simulate them suitably in the approximate analytical theory. The theory is not expected to be exact anyway simply because it is intended for use with various geometries of the inlets, the resultant velocity distributions in which are impossible to predict by a simple analytical approach.

An example of computation results is presented in Fig. 4. It shows the extent of the recirculation bubble for the basic $\varphi = 4.041$ geometry obtained in both series A and series B. The nozzle flow rate in these solutions remained constant—as documented by the constancy of the nozzle exit Reynolds number Re_b.

The value of the ratio μ_e was varied by changing the central main flow rate. In both computation series, all runs were performed up to solution convergence, the criterion being relative residual magnitudes less than 10^{-4} for all computed variables.

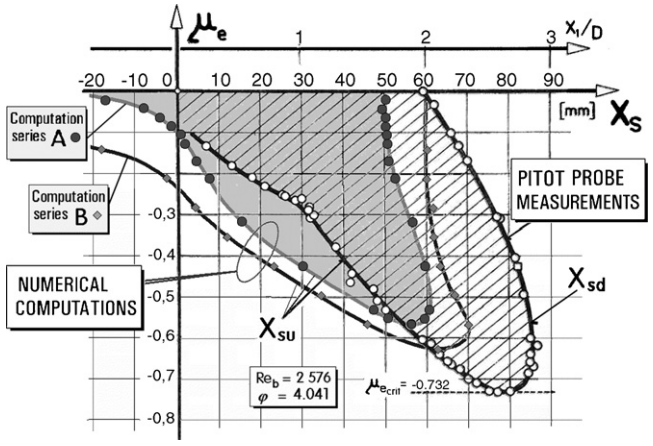

Fig. 4. Experimentally determined as well as computed locations X_s of the upstream and downstream stagnation points S_u and S_d in the basic $\varphi = 4.041$ case as in the experimental data of [4]. They depend on flow ratio μ_e (defined in Eq. (1)). As the relative wall-jet intensity decreases, the recirculation bubble moves downstream and its size diminishes.

The general character of the dependence in Fig. 4 agrees with the character of the dependence obtained in the only available experiment [4]. There is, however, not an exact agreement and, indeed – indicative of the difficulties encountered in these types of flows – also the two computation series results series do not mutually coincide. Of course, an exact coincidence could not be expected in view of the differences in their discretisation grids. There is a better agreement with the experiment for the series B computations, perhaps due to their finer grid—though the use of different solver versions should not be forgotten. Considering the already mentioned problem of unreliability of the Pitot probe measurements in these flows, the experimental data are not very reliable, either. It would be surprising to find an exact agreement with the experiment. This was, after all, not asked for. What is really important for the present purpose is the qualitative agreement in the character of the flowfield in all three approaches—and vindication of the qualitative explanation hypotheses of Tesař [4] and Markland [5].

7. The critical state at location *Y*

The main interest when evaluating the computation results concentrated on the three locations, the inlets X_1 and X_2 into the control volume and the outlet *Y* at its exit end. Of them, the location *Y* in the critical regime is the most interesting and unusual. The exit plane there contains the extraordinary zero-velocity point resulting from coincidence of two stagnation points. It is a surrounded everywhere by positive velocity flows.

The first objective was to find the position of this special point. The results (together with a schematic representation of the expected velocity profiles) presented in Fig. 5 show that the position is governed by a surprisingly simple law. This result was of importance for identification of the relative length σ_S as defined in Eq. (12) and used in Eq. (19).

The next objective was evaluation of the velocity profile shape in *Y* and then the value of the shape parameter H_Y. An extremely simplistic approximation to the profile with zero-velocity on the axis, is the linear conical velocity distribution neglecting the boundary layer at the wall, with velocity growth from the axis towards the walls from the zero value at the centre. Integration of this profile leads to shape parameter value $H_Y = 9/8$, perhaps surprisingly not so much different from the uniform profile value $H_Y = 1$ as one might be prepared to expect for such an unusual shape. However, the real profile, because of the character of the two co-incident stagnation points and the continuity condition, must posses zero radial gradient $\partial w_1/\partial X_2$ on the axis. The linear profile fails to meet this requirement

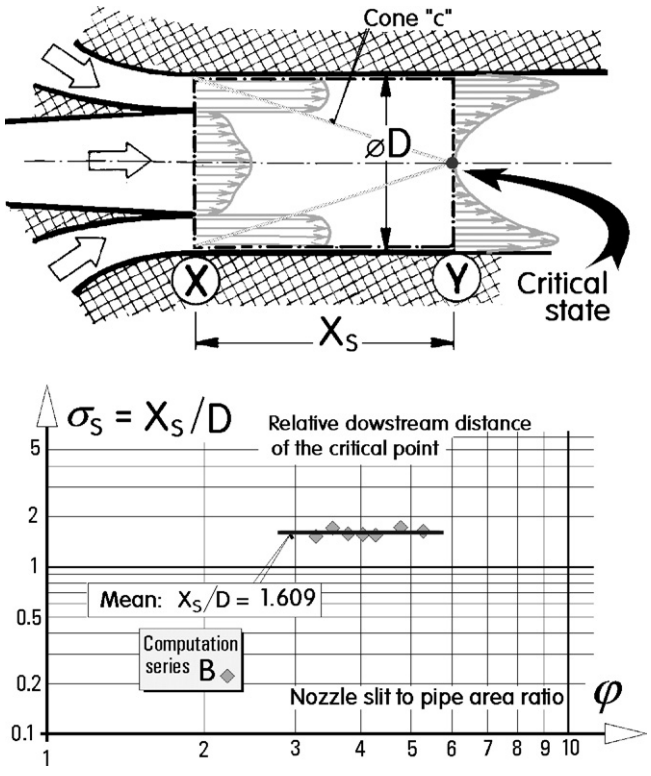

Fig. 5. The computations indicate that when the pipe diameter *D* is increased (resulting in an increase of the area ratio φ), the critical stagnation point in (*Y*) is located at the vertex of the cone *c*, which retains its constant vertex half-angle arctg $1/\sigma_s$.

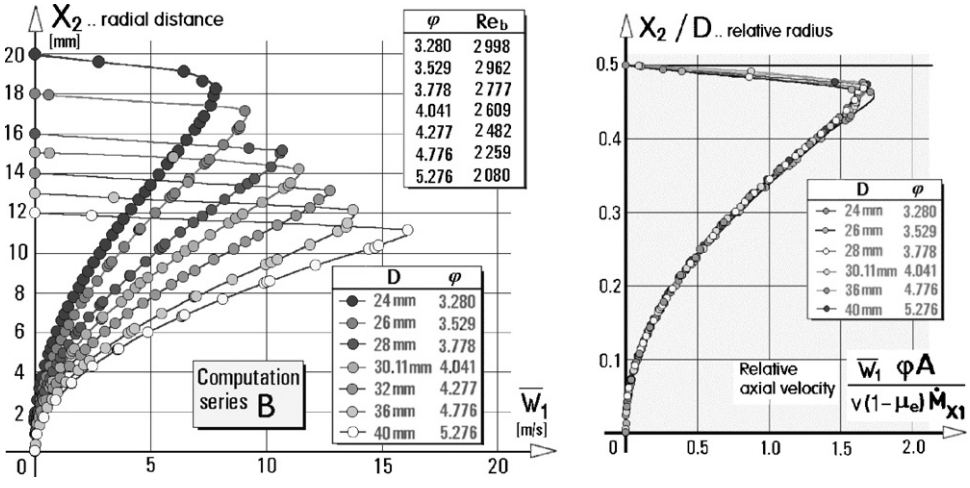

Fig. 6. Time-mean axial velocity profiles in the critical location obtained by the numerical flowfield computations for the seven investigated geometries that differ in the diameter *D* (and consequently in area ratio φ). When re-plotted in the relative co-ordinates at right, the profiles exhibit a remarkable mutual similarity.

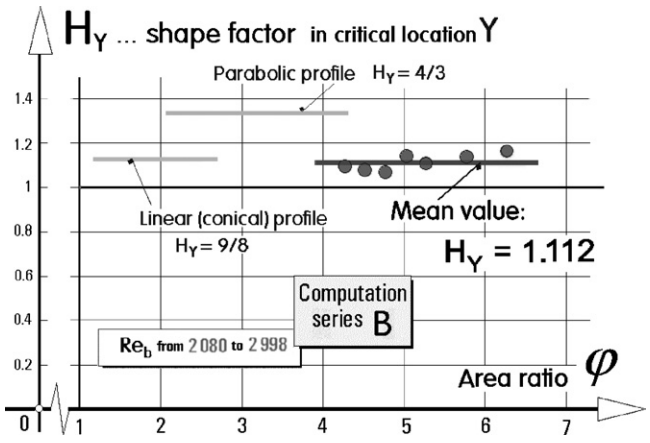

Fig. 7. The shape factor values obtained by integrating computed profiles compared with simple approximations.

and cannot be a realistic approximation. The simplest shape meeting the condition is the "inverted parabolic" velocity profile with velocity increasing quadratically from the zero value on the axis. For this approximation, again neglecting the wall boundary layer, the momentum flow rate integration results in shape factor magnitude $H_Y = 4/3$. The velocity profiles obtained by the CFD solutions are shown in Fig. 6. The remarkable feature of these profiles is their mutual similarity. They are actually very well approximated by the quadratic parabolic distribution, apart from the near-wall region where there is the quite pronounced boundary layer. In the relative co-ordinates (with the axial velocity $\bar{w}_1$ in Fig. 6 non-dimensionalised by relating it to the velocity of the equivalent uniform profile) they collapse into practically a single universal curve. A systematic dependence of the boundary layer thickness on Re may be expected but, unfortunately, the discretisation grid there was not fine enough to provide a reliable conclusion. The consequent scatter in the value of the highest velocity in the profile (on which the momentum flow rate integral is particularly sensitive) has led also to the scatter of the evaluated values of the shape factor H_Y in Fig. 7. These were computed from the definition Eq. (10) in which the momentum flow rate $\dot{W}_Y$ was evaluated by integration of the square of the computed velocity. The sensitivity to the peak values in the velocity profile is apparent in Fig. 7 from the comparison with the parabolic approximation, which neglects the presence of the boundary layer and has at the wall higher peaks.

Considering how unusually shaped are the discussed profile shapes, the H_Y values in Fig. 7 are remarkably near to the uniform profile value $H_Y = 1$, from which the results differ by an amount commensurate with the scatter caused in the numerical flowfield computations by irregularity of the used unstructured grid with the rather abrupt localised effect of the refinements.

8. The annular nozzle inlet X_1

Nozzle exit profiles in general are known to be fairly uniform [9]. Convergence of streamlines in the nozzle contraction tends to produce slightly concave bicuspid profiles with maxima near the walls, but this is countered by velocity decrease near the walls due to the boundary layer. In typical nozzles at reasonably high Reynolds numbers the wall boundary layers are usually very thin.

In the present case, the wall-jet issues from an unusual nozzle with contraction spread over a long stream-wise distance, Fig. 2. As a result, there is ample opportunity for the shear effects to produce thicker than usual boundary layers and rounding of the profile "corners". Because the nozzle slit is very narrow compared to the overall dimensions of the computation domain, the numerical computations of the nozzle flow tended to be less well resolved. Initial discretization grid produced by software GAMBIT was rather coarse there and though subsequent automatic refinements divided some cells into smaller ones, the effect was distributed rather irregularly. The uneven distribution of the data points is apparent in the four examples of the annular nozzle exit profiles shown in absolute co-ordinates in Fig. 8. The diagram shows the complicating variations of Reynolds number Re_b, computed from the nozzle width b and the maximum velocity in the exit cross-section, which – as mentioned above – decreased with increasing pipe diameter D. There did not seem to be a recognisable systematic trend, the computed profiles again exhibiting enough mutual similarity for common representation by the fourth-order polynomial fit curve. Indeed, with a single exception, the momentum flow rate $\dot{W}_{X_1}$ evaluated by direct integration of the computed profiles in Fig. 9 did not differ significantly from the values obtained by integration of the fitted polynomial. The resultant shape parameter $H_{X_1} = 1.116$ seems to be a reasonably accurate result. Somewhat surprisingly, this value is nearly the same as that evaluated for H_Y (Fig. 7).

9. The diffuser-shaped central inlet X_2

The last of the investigated velocity profiles, the one in the central, main flow inlet X_2 into the control volume, is rather exceptional. In contrast to the other profiles at X_1 and Y, which exhibit similarity (Figs. 6 and 8) their plots in the relative co-ordinates varying very little with the changes in the area ratio φ, the profiles at X_2 vary very much. This is not surprising, since the changes of φ are associated with changes of the model geometry. Because the variation of φ in the model was achieved by moving radially the insert part (Figs. 1 and 2), which introduces the protective flow, for small φ values the insert leaves only a small-diameter central inlet channel. Immediately upstream from the control volume, the transition from this channel to the exit is shaped as a conical diffuser. Its divergence apex half-angle $3°15'$ is small, ensuring the flow does not separate from diffuser wall. At the exit of such diffusers the velocity near the wall is slow and the flow concentrates into the central high-velocity peak. This concentration depends on the length of the diffuser. It is most pronounced if the diffuser is long.

If the conical wall is shifted radially, the resultant diffusers are geometrically different. For large φ (i.e. for small annular nozzle exits) the inlet part is relatively short and also small and relatively unimportant is the diffuser. On the other hand, for small area ratio φ the diffuser is long, with large area increase in the stream-wise direction. The computed velocity profiles are in agreement with these general expectations. Three profile

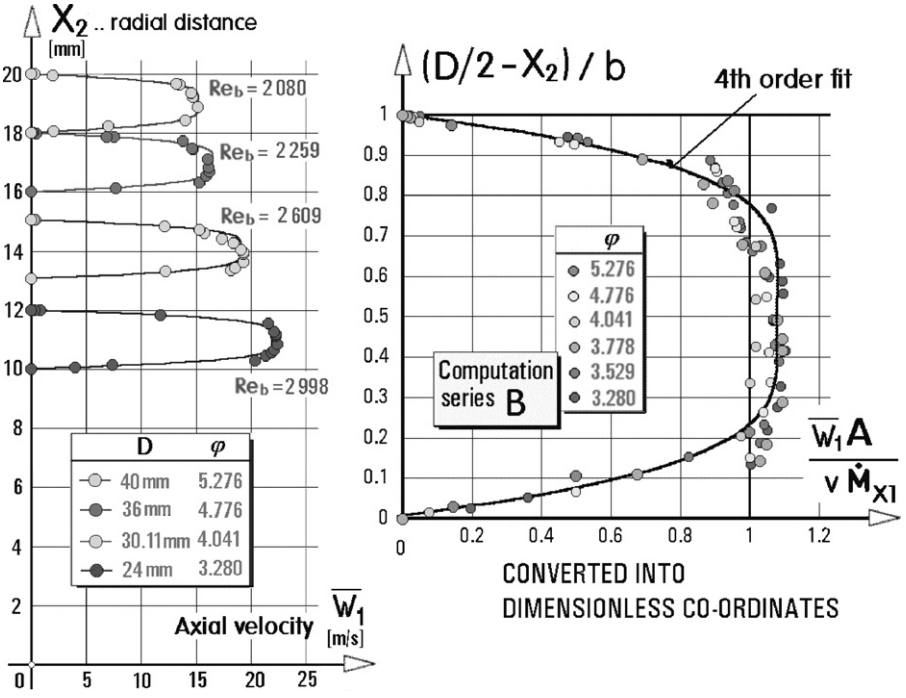

Fig. 8. Four examples of the computed velocity profiles in the X_1 exits of the wall-jet nozzles with smoothed fourth-order polynomial representations (lines) at left and cumulative plotting of the axial velocity profiles in relative co-ordinates at right. The considerable scatter is not surprising for what is actually a fine detail of the flowfield.

examples, for small, medium, and large φ within the range of the investigated geometries, are plotted in Fig. 10. A certain tendency towards the similarity is found only at the high φ end of the range, where the central channel is of large cross-section. The influence of the relatively short diffuser is far less pronounced than for small φ. It should be noted in Fig. 10 that for large φ the profiles change only little with varying φ.

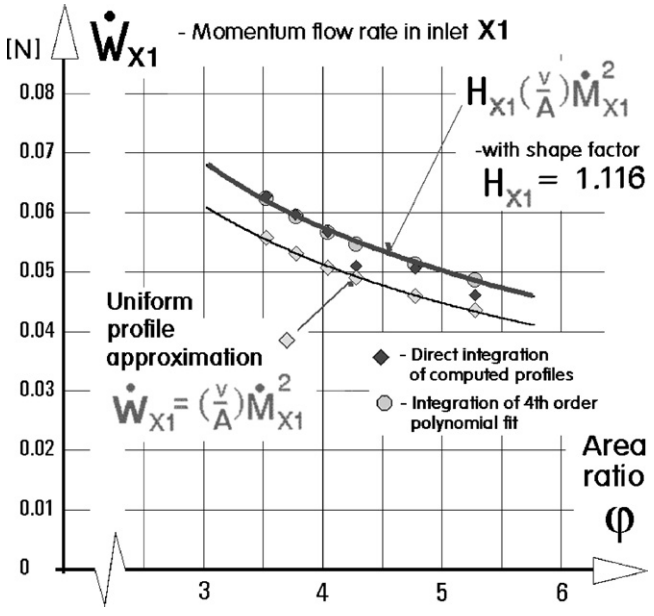

Fig. 9. Values of the nozzle exit momentum flow rate $\dot{W}_{X_1}$ obtained by integration of the computed velocity profiles are reasonably fitted by the curve assuming a constant value of the shape parameter H_{X_1}.

The computed velocity profiles were again integrated to obtain the axial momentum flow rate $\dot{W}_{X_2}$. This was then compared with the value for the uniform shaped profile, Eq. (9). The resultant the shape parameter values are H_{X_2} plotted in Fig. 11. The two different characters of the dependence on φ discussed above are clearly recognisable. At large φ, where the velocity profiles in Fig. 10 tend to be more flat and nearly similar, the shape parameter H_{X_2} values are only slightly above 1.0 and do not vary significantly with φ. This is changed at low φ, where the central high-velocity peak in Fig. 10 becomes the dominant feature. Its high velocity values contribute to the much higher values H_{X_2}, growing rapidly with decreasing area ratio φ. For the purposes of working with this dependence, the fourth-order polynomial shown together with the data points in Fig. 11 was fitted to the values. This fit is acceptable for the further operation with these results, but not the best choice at high φ, where its order is too low to represent well the near-constant, asymptotic character.

10. The wall friction

The wall friction term – the last term on the right-hand side in Eqs. (15) and (19) – represents the effect of the wall shear stress on the pipe walls, along the outer boundary of the control volume (Fig. 5). In the computations, the local wall shear stress τ_w is available directly, being a value reported by FLUENT. What is needed for the control volume balance is the overall friction coefficient c_f according to Eq. (13), obtained by integration along the wall and plotted in Fig. 12. While in other flows the friction forces are usually small, in the present case the c_f values are very high because of the very high velocity gradient at the wall,

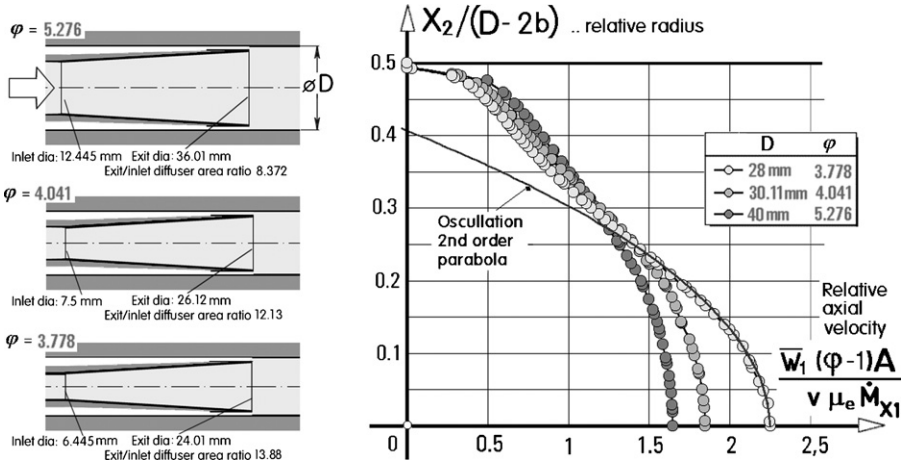

Fig. 10. Velocity profiles in the central inlet X_2 into the control volume. Due to the conical diffuser character immediately upstream – more pronounced at small φ – the profiles there are characterized by a high-velocity central peak, exceeding considerably the mean velocity value.

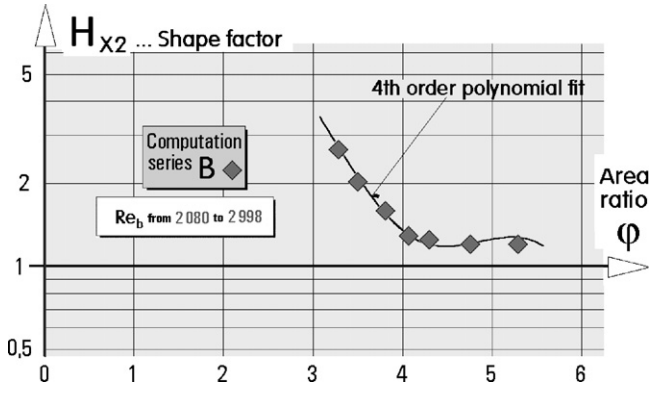

Fig. 11. The shape factor H_{X_2} evaluated by integrating the computed velocity profiles in the inlet location X_2. For large area ratio φ (large diameter D) the diffuser effect is weak, H_{X_2} is nearly constant and only slightly larger than 1.0, similarly as in the other two locations X_1 and Y. On the other hand, with the conical wall nearer to the axis in the small D cases produces velocity profiles with sharp central peaks (Fig. 10) resulting in rising H_{X_2} with decreasing φ.

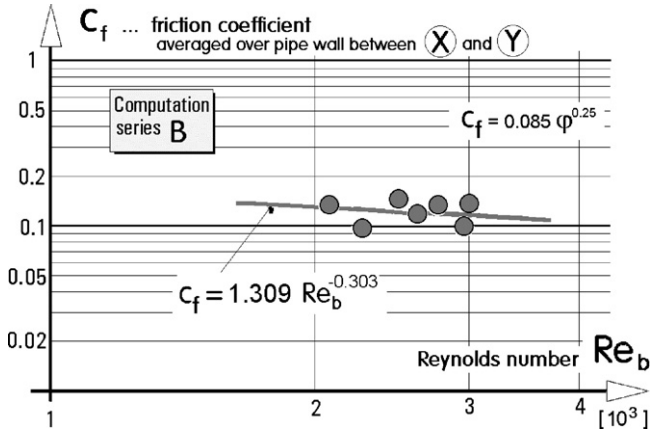

Fig. 12. Reynolds number dependence of the wall friction coefficient c_f. The values are much higher than in developed pipe flows, in agreement with the fact that they are evaluated for high-speed flow immediately adjacent to the pipe wall.

caused by the presence there of the high-speed protective jet. This, after all, is why the definition Eq. (13) relates τ_w to the wall-jet generating nozzle flow rate $\dot{M}_{X_1}$. Unfortunately, wall shear is generally among the least reliable computational results. This is why there is the large scatter in Fig. 12, despite the smoothing by the integration procedure. The power law fit shown there suggests a rise with increasing area ratio φ, no doubt reflecting the common tendency of friction coefficients to decrease with increasing Reynolds number.

11. Pressure rise in the axial flow

Euler number Eu_M, the last quantity needed for the control volume force balance Eq. (14), characterises the pressure rise ΔP in the flow direction. This jet-pump pressure increase [4] is due to the decrease of the overall momentum flow rate between the planes X and Y. To compute it requires only a simple application of the energy balance Bernoulli equation along the pipe axis. The integration path there is actually a streamline along which this equation may be legitimately applied. Contrary to initial expectations, the extraordinary character of the velocity field at and near to the critical state Y is not reflected in any special feature on the pressure rise curves. In Eq. (14) the non-dimensionalisation of the pressure term is needed in the form relating it to $\dot{M}_{X_1}$ and this is why the nozzle flow is used in the final Euler number definition in Eq. (11). In fact the jet-pumping effect pressure rise takes place in the pumped central flow between X_2 and Y. Unfortunately, because of the complexity of the velocity profile in X_2, the velocity is not simply related to the mass flow rate $\dot{M}_{X_2}$ passing through the central inlet. Its relation in Eq. (11) to $\dot{M}_{X_1}$ based on the assumption of uniform profiles is even more complicated.

For successful simple theory of the device, the Euler numbers should preferably be constants near to 1.0. As seen in Fig. 13, this is not the case, in particular at the low φ end of the investigated range, where the distributions tend to deviate quite strongly from the ideal value. Fortunately, as shown in the next paragraph, the pressure term is generally smaller than the other terms in the momentum balance Eq. (14). The difficulties in estimating its value thus do not endanger the predictions of the theory.

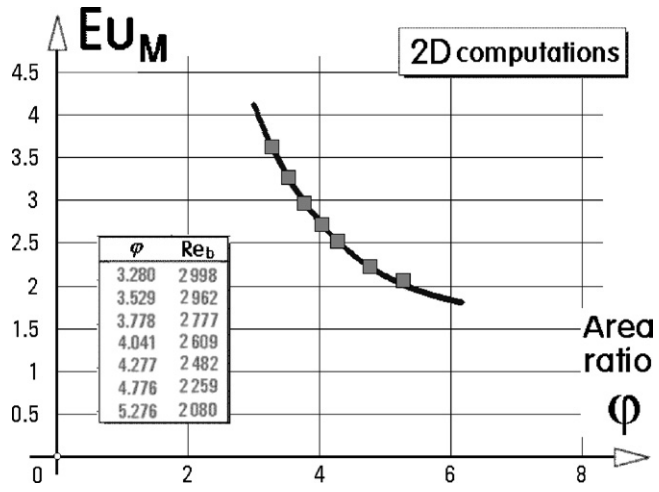

Fig. 13. The values of the Euler number Eu_M characterizing the pressure at the control volume outlet (Y) decrease with increasing area ratio φ rather rapidly. This is due to the disappearance of the central velocity peak at X_2 velocity profile, Fig. 10.

12. Resultant predictions for the flow reversal

The sought-after dependence Eq. (4) determining the critical flow reversal is determined by the dimensionless Eq. (15) which, apart from the independent variable – the area ratio φ – contains the introduced dimensionless parameters. These were evaluated one by one in preceding paragraphs by analysis of experimental and computed data for the geometry of Fig. 2 and its variants having a different area ratio φ. The present theory of the reversal would be perfect if the parameters were constant and easily predictable. This was found to be the case for the correction parameters for nozzle momentum rate term H_{X_1} and for the critical point momentum rate H_Y. They are practically constant (the velocity profiles in these locations meet the similarity condition) and their magnitude may be well characterised as being ~10% higher than the ideal value 1.00. This deviation may be even neglected altogether for first estimates.

Because of the character of the central inlet, which the design constraints necessitated to shape as a conical diffuser, the results are less satisfactory in the case of the main flow inlet momentum rate correction parameter H_{X_2}. It behaves acceptably for large area ratio φ values, where the diffuser effect is less pronounced. The value there is higher than the ideal 1.00, nevertheless it is nearly constant and reasonably predictable. For $\varphi < 4$ the central peak in the velocity profile becomes the dominant feature and H_{X_2} values increase beyond a simply predictable magnitude. The theory then becomes less simple and perhaps less useful.

The friction term is determined by the values c_f and σ_S. These are acceptably constant (for the former it is possible to take into the account its predictable small decrease with increasing Reynolds number) but the numerical values are difficult to estimate so that the present results (perhaps improved upon in future by analysis of another case) are invaluable.

Finally, perhaps the least satisfactory is the pressure term, for which the Euler number as introduced by Markland [5] is large, inconstant, and generally difficult to predict.

The parameters, however, do not have the same weight in the solved problem. It is instructive to consider the magnitudes of the individual terms in the force balance Eq. (15). They are plotted in Fig. 14 as two diagrams, separately for the left-hand and right-hand side of Eq. (15). It is apparent that, fortunately, the force balance is dominated by the two well behaving terms, the nozzle momentum rate term and the critical point momentum rate term. On the other hand, the main flow momentum term and the difficult to predict pressure rise term are the least important.

The ultimate result – the solution of the quadratic Eq. (16) – is plotted together with the data points for the seven computed cases in Fig. 15. What is important there is mainly the qualitative character of the solution, as it is assumed that the quantitative aspect will be improved upon in future when other experimental or more reliable numerical data will become available. An interesting fact evident from Fig. 15 is that at high values of the area ratio φ, where the diffuser effect in the inlet X_2 ceases to be important, the condition becomes self-similar. The critical state becomes fully determined by the ratio of the two velocities,

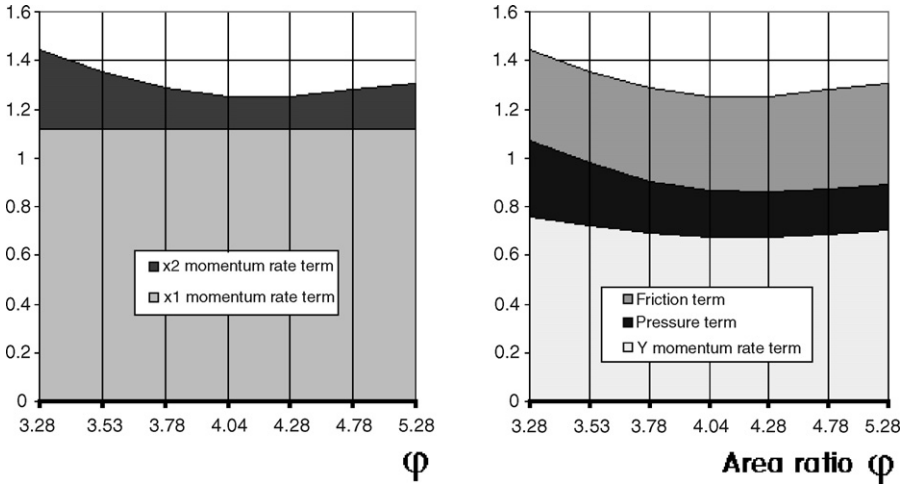

Fig. 14. Magnitudes of individual left-hand and right-hand terms in the non-dimensionalised force balance Eq. (15) in the seven numerically computed cases having different area ratios φ. These diagrams provide an idea about the relative importance of the force balance components acting on the investigated control volume.

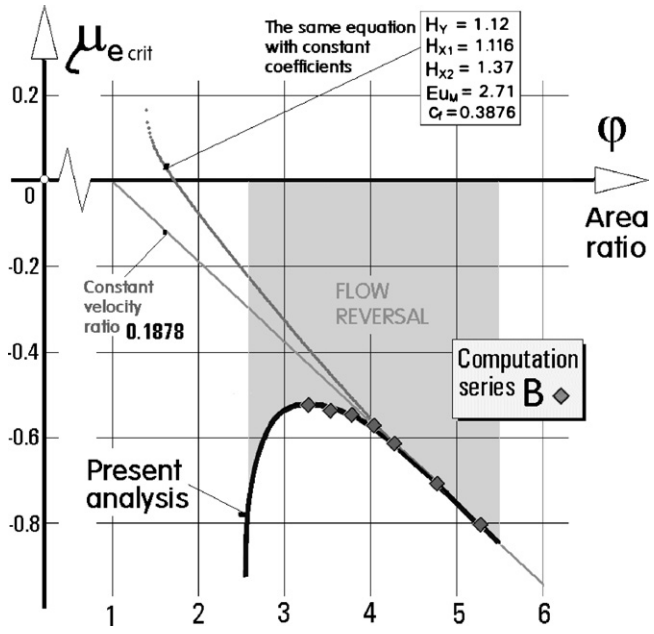

Fig. 15. The result of the analysis predicted dependence of the critical flow rate on the pipe to nozzle area ratio compared with the results of the computations.

w_{X_1}—the nominal (bulk) in the inlet X_1 and w_{X_2} in X_2:

$$\frac{w_{X_2}}{w_{X_1}} = \frac{\dot{M}_{X_2}}{(\varphi - 1)\dot{M}_{X_2}} = 0.1878 \tag{20}$$

the solution of Eq. (14) then approaches the linear asymptotic dependence:

$$\mu_{\mathrm{e\ crit}} = 0.1878(\varphi - 1) \tag{21}$$

Another interesting conclusion from Fig. 15 is the importance of the inconstancy of the introduced parameters H_{X_2}, Eu_{M} and c_{f}, all three being dependent on the area ratio φ. Ignoring the dependence and fitting a constant parameter value evidently leads to a solution in agreement with the straight line asymptote Eq. (21) at high φ but deviating from it for small φ values to the very opposite side than the deviation found in the constant-values computations.

An interesting test of the self-similarity observed at high values of the area ratio φ is shown in Fig. 16. The quantity plotted there as a function of φ for the investigated seven critical states is essentially the Thring–Newby number [1] used as the criterion of similarity in coaxial burners. It was adapted for the present case by taking as the primary (driving) flow parameters those of the annular wall-jet (rather than the central jet in the original version). The value of this parameter is indeed constant in for those four critical states in which the present investigations (Fig. 15) discovered the desirable invariance.

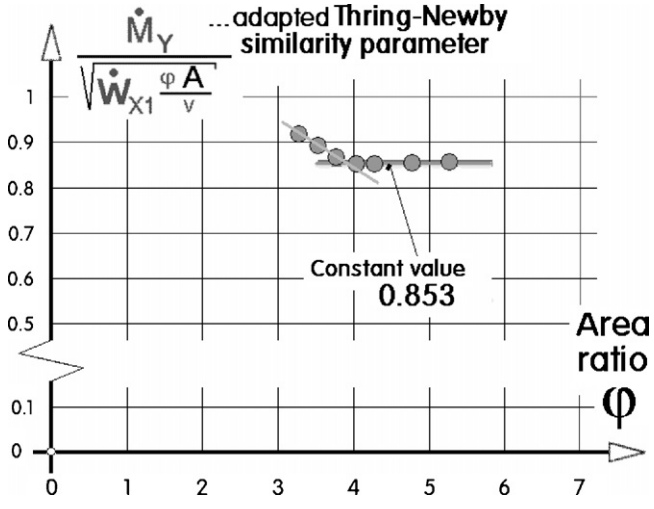

Fig. 16. The Thring–Newby number adapted for the present case of the annular primary nozzle evaluated in the seven investigated critical states. At high ($\varphi > 0.4$) values of the area ratio this similarity parameter is a constant.

13. Conclusions

Pipe flows with the protective "guard" wall-jet can find numerous applications in chemical engineering, whenever it is desirable to prevent a contact of the fluid flow from the pipe wall. The wall-jet, however, can generate a stationary recirculation bubble, leading to flow reversal on the axis. While originally causing a problem in the detecting and sensing applications, the phenomenon may be useful, e.g. to stabilise a location of a chemical reaction zone in the pipe without any mechanical baffles obstructing the pipe internal space.

Knowledge of the critical conditions beyond which the flow reversal must be expected is crucial for designing such devices. Numerical flowfield solutions, while a helpful tool for checking the final configuration, do not provide a proper help in the initial design stages when the designer has to choose the flow rates and the basic geometric parameter, the area ratio φ. The optimum can be arrived at by performing a series of solutions with alternative geometries, but this is expensive and time consuming. The simple momentum rate balance theory presented here provides a useful guideline.

Values of the "constants" of this model were identified by analysis of earlier experimental data and a series of numerical solutions. Neither the experiment nor the computations themselves were perhaps perfectly reliable – and may be certainly improved upon – but the qualitative conclusions arrived at are interesting. The model can predict the existence of the flow reversal. Several of the introduced corrective factors introduced – H_{X_1}, H_Y, H_{X_2}—the latter only within the range of the similarity at high φ – were found to have values sufficiently near to 1.0 to permit reasonable guesses based on the crude assumption of uniform velocity profiles. In the similarity regimes, existence of flow reversal is predicted by very simple constant velocity ratio rule.

In the investigated case, the similarity is lost at low φ values. The cause for this are the consequences of the wall-jet nozzle placed inside the pipe (Fig. 1). At small φ this destroys the geometric similarity, contracting and deforming the main inlet flow so much that the similarity assumption ceases to be valid. This regime is revealed by inconstancy of (adapted) Thring–Newby number.

The theory remains useful, however, even beyond the similarity limit. The information painstakingly accumulated about the character of the flowfield and the resultant magnitudes and variations of the parameters can provide a useful guidance.

Acknowledgments

The author was given the opportunity to use the White Rose computational resources during his stay at the University of Sheffield, which was supported by EPSRC grant to Prof. W. Zimmerman. Author is also grateful to Prof. E. Markland who provided him with his study [5] on which the basic ideas of the present analysis were founded.

References

[1] M.W. Thring, M.P. Newby, Proceedings of the Combustion Length of Enclosed Turbulent Jet Flames Fourth Symposium (International) on Combustion, Williams and Wilkins, Baltimore, 1953, p. 789.

[2] A. Craya, C. Curtet, Sur l'évolution d'un jet en espace confiné, Comptes-Rendus Acad. Sci. 24 (1955) 611.

[3] M. Barchilon, R. Curtet, Some details of the structure of an axisymmetric confined jet with backflow, Trans. ASME J. Basic Eng. 86 (4) (1964) 777.

[4] V. Tesař, Vývoj plynové kyvety, Etapa I: Příprava řešení (1978), Etapa II: Experimentálni vyšetřování proudění v kyvetě (1979), Etapa III: Transport kontaminantu napříč ochranným filmem (1980), in Czech, Research Reports written at Faculty of Mechanical Engineering CVUT, Prague, for the Nuclear Research Institute, Czech Republic, 1978–1980.

[5] E. Markland, Flow Reversal in an Annular Ejector, Unpublished Memorandum, University College Cardiff, Department of Mechanical Engineering and Energy Studies, 1986, 10 pp.

[6] F. Risso, J. Fabre, Diffusive turbulence in a confined jet experiment, J. Fluid Mech. 337 (1997) 233–261.

[7] X.-Q. Chen, M. Renksizbulut, X. Li, Interaction of a particle laden gaseous jet with a confined annular turbulent flow, Particle Particle Syst. Charact. 18 (2001) 120–133.

[8] P.J. Foster, J.M. MacInnes, F. Schubnell, Approximate similarity of confined turbulent coaxial jets, Trans. ASME, J. Fluids Eng. 123 (2001) 707.

[9] V. Tesař, Nozzle characteristics—the boundary layer model, Hydraul. Pneumat. XXIV (3) (2004) 35–43 (ISSN: 1505-3954).

[10] A. Revuelta, C. Martínez-Bazán, A.L. Sánchez, A. Liñán, Laminar Craya–Curtet jets, Phys. Fluids 16 (1) (2004) 208–211.